Biosensors and Bioelectronics 57 (2014) 269–275

Contents lists available at ScienceDirect

Biosensors and Bioelectronics

journal homepage: www.elsevier.com/locate/bios

Biomolecule-adsorption-dependent piezoelectric output of ZnO nanowire nanogenerator and its application as self-powered active biosensor

Yayu Zhao [a], Ping Deng [a], Yuxin Nie [a], Penglei Wang [a], Yan Zhang [b,c], Lili Xing [a,*], Xinyu Xue [a,b,**]

[a] College of Sciences, Northeastern University, Shenyang 110004, China
[b] Beijing Institute of Nanoenergy and Nanosystems, Chinese Academy of Sciences, Beijing 100000, China
[c] Institute of Theoretical Physics, Lanzhou University, Lanzhou 730000, China

ARTICLE INFO

Article history:
Received 30 October 2013
Received in revised form
24 January 2014
Accepted 10 February 2014
Available online 19 February 2014

Keywords:
Biosensor
Nanogenerator
ZnO
Self-powered
Piezoelectric

ABSTRACT

Self-powered active biosensor has been realized from ZnO nanowire (NW) nanogenerator (NG). The piezoelectric output generated by ZnO NW NG can act not only as a power source for driving the device, but also as a biosensing signal. After immersing in 10^{-3} g ml^{-1} human immunoglobulin G (IgG), the piezoelectric output voltage of the device under compressive deformation decreases from 0.203 ± 0.0176 V (without IgG) to 0.038 ± 0.0035 V. Such a self-powered biosensor has higher response than transistor-type biosensor (*I–V* behavior). The response of self-powered biosensor is in a linear relationship with IgG concentration (logarithm, 10^{-7}–10^{-3} g ml^{-1}) and the limit of detection (LOD) on IgG of the device is about 6.9 ng ml^{-1}. The adsorption of biomolecules on the surface of ZnO NWs can modify the free-carrier density, which vary the screening effect of free-carriers on the piezoelectric output. The present results demonstrate a feasible approach for actively detecting biomolecules by coupling the piezotronic and biosensing characteristics of ZnO NWs.

1. Introduction

Biosensors for detecting biomolecules have great applications in medical diagnostics, food/nutrition industry and environmental monitoring (Song et al., 2010; Mello and Kubota, 2002; Dennison and Turner, 1995). In recent years, semiconducting metal oxide nanowires (NWs), such as ZnO, SnO_2 and In_2O_3, have been confirmed as good candidates for highly-sensitive biosensing due to their high surface-to-volume ratio (Yeh et al., 2009; Hu et al., 2010; Li et al., 2010; Curreli et al., 2005). In particular, ZnO NWs for biosensing have been intensively investigated because of their biological friendliness and low cost. The biomolecules adsorbed on the surface of ZnO NWs can change the conductance of the NWs by modifying the surface charges and states (Cui et al., 2001; Patolsky and Lieber, 2005; Lieber, 2003), disturbing the gate potential (He et al., 2007; Heller et al., 2008; Gui et al., 2007), changing the gate coupling (Besteman et al., 2003), and/or altering the carrier mobility (Maroto et al., 2007). Thus the adsorption of target biomolecules on ZnO NWs is equivalent to adding a potential gating that leads to a change of electron density within the n-type ZnO NW field effect transistor (FET) (Dong et al., 2010). Additionally, ZnO NWs with wurtzite structures have attracted world-wide attention due to their high piezoelectric output under externally applied deformation, and ZnO NW piezoelectric nanogenerator (NG) has been integrated in various self-powered nanosystem (Wang and Song, 2006; Xu et al., 2010; Zhang et al., 2012b). When the *c*-axis of ZnO NW is under external strain, a piezoelectric field can be created on the surface that can not only drive the electrons in the external circuit flowing forward and back (the output of NG), but also make the carriers in ZnO NWs migrate and partially screen this piezoelectric field (piezotronics effect) (Pan et al., 2011; Yang et al., 2008). If the biosensing and piezotronics properties of ZnO NWs can be coupled into a single physical process then a new type of self-powered active biosensor can be realized through its biomolecule-adsorption-dependent piezoelectric output.

In this paper, new self-powered active biosensors have been realized from ZnO NW piezoelectric NG with bio-functionalization. The piezoelectric output of the ZnO NW NG acts as both the

* Corresponding author. Tel.: +86 24 8368 7658.
** Corresponding author. Tel.: +86 24 8368 7658.
E-mail addresses: xingrenyier@sina.com (L.L. Xing), xuexinyu@mail.neu.edu.cn (X.Y. Xue).

http://dx.doi.org/10.1016/j.bios.2014.02.022
0956-5663

energy source and biosensing signal. The piezoelectric output response of ZnO NG to human immunoglobulin G (IgG) has been studied, aiming to explore the mechanism of coupling the biosensing and piezotronics properties of ZnO NWs. As the concentration of IgG increases, the piezoelectric output of the device decreases. The experimental data demonstrate that the ZnO NG can act as a self-powered biosensor for actively detecting biomolecules without requiring external electric power. Our results can stimulate a new direction for the development of the next generation of biosensors and will further expand the scope for self-powered nanosystems.

2. Experimental details

2.1. Synthesis and functionalization of ZnO nanoarrays

Vertically-aligned ZnO NW arrays were firstly synthesized by a wet-chemical method (Li et al., 2008). All chemicals (purchased from Sinopharm Chemical Reagent Co. Ltd.) were analytical-grade reagents and used as purchased without further purification. Prior to growth, a piece of Ti foil (the thickness is 0.1 mm) as the substrate was cleaned with deionized water and alcohol, respectively, then dried at 60 °C. 0.416 g of $Zn(NO_3)_2 \cdot 6H_2O$ was dissolved into 38 ml of deionized water. After magnetically stirring for 10 min, 2 ml of $NH_3 \cdot H_2O$ was added into the solution drop by drop. Then the Ti foil was immersed into the solution, and the reaction flask was sealed. After being kept at 70 °C for 24 h, the substrate was removed from the solution, rinsed with deionized water, and dried at 60 °C.

Then the surface of ZnO NWs was modified with gold nanoparticle–anti-Immunoglobulin G (Au NP–anti-IgG) conjugates. Colloidal Au has been recognized as a versatile and efficient template for the immobilization of biomolecules due to its easy preparation, relatively large surface and good biocompatibility (Cai et al., 2001; Chen et al., 1998; Rembaum and Dreyer, 1980). The colloidal Au can not only enhance the amount of antibodies immobilized on the surface of ZnO NWs, but also preserve the activity of the immobilized biomolecules. Anti-IgG molecule is also anchored to the surface of ZnO NW through Au NPs (Mao et al., 2010). 0.1 ml of Au NP–anti-IgG colloidal solution (purchased from Ted Pella Inc.) was dropped upon the ZnO NW arrays, and then incubated in the fume hood for 1 h. After that, the sample was modified with block buffer (BB) (0.1% Tween 20 (purchased from Ted Pella Inc.), 0.1% fish gelatin (purchased from Ted Pella Inc.), and 1% bovine serum albumin (BSA) (purchased from Sigma-Aldrich Co. LLC.)). It was reported that BB could efficiently block the nonspecific binding of IgG (purchased from Sigma-Aldrich Co. LLC.) to the samples (Mao et al., 2010). Thus, treating the sample with BB can effectively diminish the undesirable response from the nonspecific binding to the sample and is necessary for the specific function of the sensor. Samples treated by BB were dried at room temperature for 2 h, and then cleaned with phosphate buffer solution (PBS) (Yu et al., 2013b).

2.2. Fabrication of the self-powered active biosensor

Finally the device is fabricated as follows: A sheet of flexible aluminum foil (0.05 mm thick) was positioned on the top of the ZnO NW arrays as the counter electrode. And two terminal copper leads were glued with silver paste on the Ti foil and Al foil for electrical measurements, respectively. Then the finished device was fixed between two sheets of Kapton board firmly. Before the measurement of self-powered biosensing, the device was immersed in a certain concentration of IgG solution for 1 h, rinsed, and completely dried at room temperature.

The design and brief fabrication process of the ZnO NG for self-powered active biosensing is shown in Fig. 1. Firstly, a piece of titanium foil as the substrate of ZnO NW arrays is pre-cleaned (Fig. 1a). Then vertically-aligned ZnO NW arrays are grown on the titanium substrate by a wet chemical method (Fig. 1b). As shown in Fig. 1c, before detecting IgG, the surface of ZnO NWs needs to be modified with Au NP–anti-IgG by a physical adsorption method. It

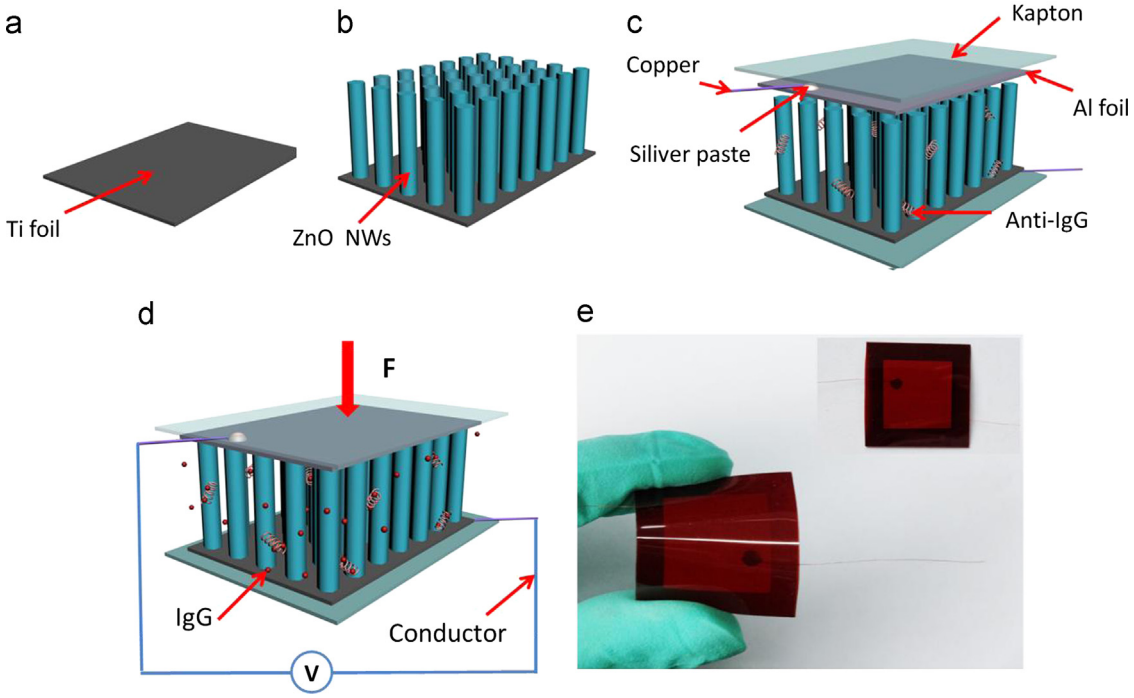

Fig. 1. Fabrication of the self-powered active biosensor. (a) A pre-cleaned Ti foil is used as the substrate. (b) Vertically-aligned ZnO NWs are grown on the Ti foil. (c) The structure design of the self-powered active biosensor after the anti-IgG being assembled onto the surface of ZnO NWs. (d) Schematic image showing the self-powered detecting of IgG. (e) An optical image of the self-powered active biosensor.

should be noted that anti-IgG antibody bound to Au NPs is immobilized on the NW surface. A layer of aluminum foil acting as an electrode is placed on ZnO NWs, and two terminal copper leads are glued with silver paste on both electrodes for piezoelectric measurements. After that, the device is tightly fixed between two sheets of flexible Kapton board as the support frames to ensure the electric contact between the aluminum foil and the NWs. It has been confirmed that flexible Kapton layers as substrates can follow the height profiles of the NW arrays and make effective contacts between the tips of NWs and electrodes (Lee et al., 2011b). When detecting IgG, the device is immersed into a certain concentration of IgG solution for 1 h to bind IgG molecules on the antibody. The device is rinsed with PBS and dried at room temperature. Then the device is tested by outside circuit and the data is collected by computer (Fig. 1d). Under applied force, the piezoelectric output of the device can act as both the energy source and the biosensing signal. An optical image of the device is presented in Fig. 1e, revealing that the NG has a length of 3 cm and a width of 3 cm, and also showing that the device is very flexible, a good feature making it efficiently convert external compressive strain into an electrical signal.

3. Results and discussion

3.1. Morphological and crystalline characterization of ZnO nanoarrays

Fig. 2a is a typical scanning electron microscopy (SEM) image of ZnO NW arrays from the top view, showing a good uniformity. The average diameter of ZnO NWs is about 200 nm. Fig. 2b is the SEM image of ZnO NW arrays from the side view, revealing that the length of the vertically-aligned nanoarrays is about 3 μm. Fig. 2c is an X-ray diffraction (XRD) pattern of ZnO NWs. The sharp diffraction peaks indicate the good crystalline quality. The peaks marked by trigon can be indexed to Ti (JCPDS File no. 44-1294) arising from the Ti substrate; the peaks marked by asterisk can be indexed to ZnO (JCPDS File no. 36-1451). As the bottom of the nanoarrays is a seed layer with multicrystal structures (as shown in Fig. 2b), the diffraction peak of (101) has high intensity. Fig. 2d is the high-resolution transmission electron microscopy (HRTEM) image of the tip region of a ZnO NW, clearly indicating that ZnO NW is single crystalline with a growth direction along the *c*-axis.

3.2. Work mechanism of self-powered active biosensor

It has been demonstrated that ZnO NWs have a high density of point defects, such as oxygen vacancies, which provide n-type carriers (electrons) for the measured conductivity (Wu et al., 2012). The output of ZnO NG is largely influenced by the carrier density inside ZnO NWs. For example, after annealing in air, ZnO NWs have fewer surface defects, resulting in less n-type carriers within ZnO NWs; the screening effect of the free carriers on the piezoelectric polarization charges is weak, thus the output of ZnO NG is high (Hu et al., 2012). Our previous report also shows that the free-carrier density at the surfaces of ZnO NWs is affected by oxidizing or reducing gas adsorbed on the surface, which greatly changes the screening of the piezoelectric polarization charges at the interface, thus affecting the piezoelectric output of the NG (Xue et al., 2013). And from previous theoretical and experimental works, the change in free-carrier density can also affect the intrinsic potential of the Schottky contact or p–n junction in piezoelectronic devices (Zhang et al., 2011, 2012a). Alternatively, the electron density of ZnO NWs can probably be affected by the adsorption of biomolecules, which can establish a local electric field and greatly change the screening of the piezoelectric field, thus affecting the piezoelectric output of the NG. In the following measurements, ZnO NG under the same strain has different piezoelectric outputs when modified with different concentrations of IgG. ZnO NG has two functions: one is as an energy source because the ZnO NWs can produce piezoelectric output power; the other is a biosensor function because the output of NG is a measure of surface adsorbed IgG.

The detailed working mechanism of the self-powered active biosensor driven by compressive strain is shown in Fig. 3. The compressive force applied on the device is 34 N at the frequency of 1 Hz. The area of the hammer for applying the compressive force is larger than that of the device. The hammer is controlled by a programed motor, and the force and frequency are constant. Thus the hammer can provide stable and uniform strain on the device

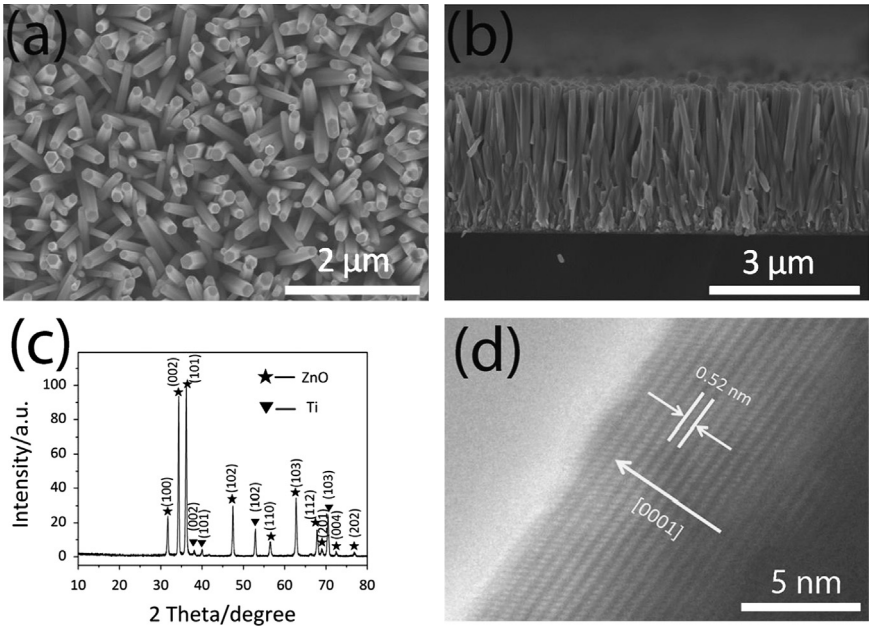

Fig. 2. (a) SEM image of ZnO NWs from the top view. (b) SEM image of ZnO NWs from the side view. (c) XRD pattern of ZnO NWs. (d) HRTEM image of the tip region of a ZnO NW.

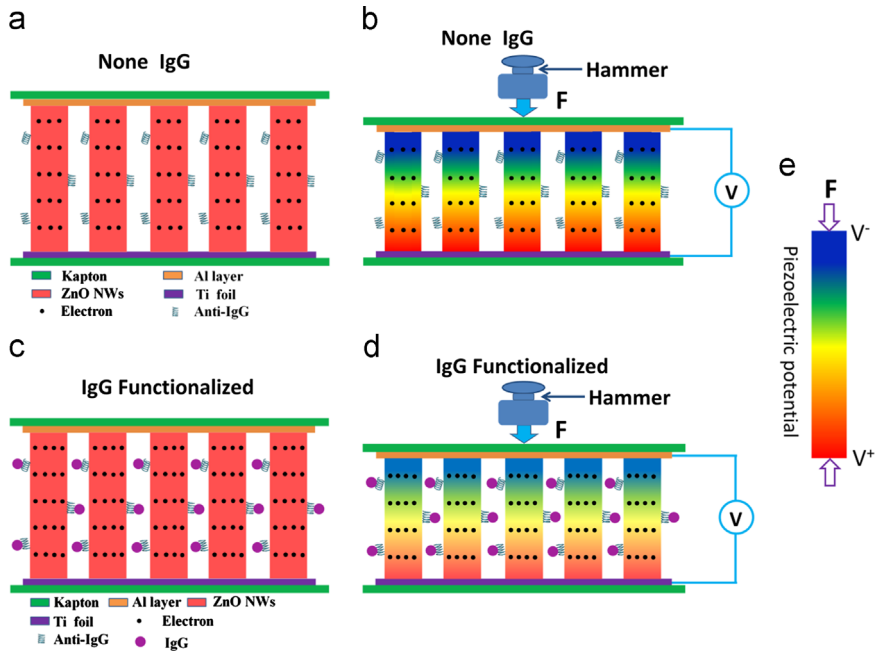

Fig. 3. The working mechanism of the self-powered active biosensor. (a) Schematic illustration of the charge–carrier density in ZnO NWs without compressive force, and the device has not been immersed in IgG solution. (b) The piezoelectric output of the device without IgG functionalization under compressive force. (c) The charge–carrier density in ZnO NWs without compressive force, and the device has been immersed in IgG solution. (d) The piezoelectric output of the device with IgG functionalization under compressive force. (e) The color scale bar represents the different piezoelectric potential.

for the experimental measurement. When testing, the two electrodes of the device are connected to a low-noise preamplifier (Model SR560, Stanford Research Systems) through coaxial lines. The data is collected by a computer through a data acquisition card. As shown in Fig. 3a and b, ZnO NWs modified with Au NP–anti-IgG have not been immersed in IgG solution. Without any compressive force, the device is in the natural state without any piezoelectric output (Fig. 3a). When an external stress is applied on the device (Fig. 3b), a piezoelectric field is created along the ZnO NWs due to the deformation of *c*-axis (Wang, 2010, 2012). Under the driving of the piezoelectric field, free electrons in the conduction band tend to flow and screen the positive ionic piezoelectric charges at one end, leaving the negative ionic piezoelectric charges alone, which reduces the piezoelectric output (Gao and Wang, 2009). As shown in Fig. 3c and d, after the device being immersed in IgG solution, IgG molecules combine with the Au NP–anti-IgG on the surface of ZnO NWs. IgG molecule contains four peptide chains (two heavy chains and two light chains) (Mao et al., 2010), and the end of the peptide chain are amino groups which are positively charged. The IgG molecules adsorbed on the surface of ZnO NWs can change the carrier density of the NWs by modifying the surface charges and states, disturbing the gate potential, changing the gate coupling, and/or altering the carrier mobility. This can be regarded as a "floating gate" effect on the conducting channel of the NWs (Pan et al., 2013). Thus the positively charged IgG is equivalent to a positive potential gate on the ZnO NWs, and this process can increase the electrons density on the surface of ZnO NWs. When the device is under a compressive strain (Fig. 3d), the piezoelectric potential is created along the ZnO NWs, and the increased carrier density of ZnO NW surface enhances the screening effect, resulting in lower piezoelectric output. As ZnO NWs have different charge–carrier densities in different concentrations of IgG, the piezoelectric output of NGs influenced by carrier density contains the biosensing information. Fig. 3e is a color scale bar that represents the different piezoelectric potentials when the device is under compressive force.

3.3. Detection of IgG using self-powered active biosensor

As shown in Fig. 4, the dependence of the piezoelectric output on the concentration of IgG demonstrates the feasible approach as a self-powered active biosensor. The room-temperature piezoelectric output voltage of one device with a size of 3 cm × 3 cm is measured by a low-noise preamplifier under the same applied strain (~0.01%, 1 Hz). The test numbers are 10, 15, 13, 11, 15 and 13 with the IgG concentrations of 0, 10^{-7}, 10^{-6}, 10^{-5}, 10^{-4} and 10^{-3} g ml^{-1}, respectively, as shown in Fig. 4a–f. The standard deviations (SD) of the piezoelectric output in each concentration of IgG is calculated, as shown in Fig. 4a–f. When the device is not modified with IgG (Fig. 4a), the piezoelectric output voltage under the compressive force is about 0.203 ± 0.0176 V. After the device being immersed in IgG solution (Fig. 4b–f), the piezoelectric output voltage decreases due to the increasing carrier density induced by the adsorption of IgG. When the concentrations of IgG solution are 10^{-7}, 10^{-6}, 10^{-5}, 10^{-4} and 10^{-3} g ml^{-1}, the piezoelectric output voltages of the device are 0.124 ± 0.0104, 0.105 ± 0.0068, 0.083 ± 0.0066, 0.064 ± 0.0048 and 0.038 ± 0.0035 V, respectively. And the relative standard deviation (RSD) ranges from 6.48% to 9.21%. The positively charged IgG is equivalent to a positive potential gate on the ZnO NWs, and this process can increase the electrons density of ZnO NWs. The increasing concentration of IgG increases the electrons density of ZnO NWs, thus the screening effect is enhanced, resulting in lowering down the piezoelectric output.

The calibration curve fits the equation $y = a + b\log_{10}x$ (with $R^2 = 0.99593$, $a = -0.0237$, $b = -0.0213$; y is the piezoelectric output voltage, x is the concentration of IgG). The response of self-powered biosensor is in a linear relationship with IgG concentration (logarithm, 10^{-7}–10^{-3} g ml^{-1}). The limit of detection

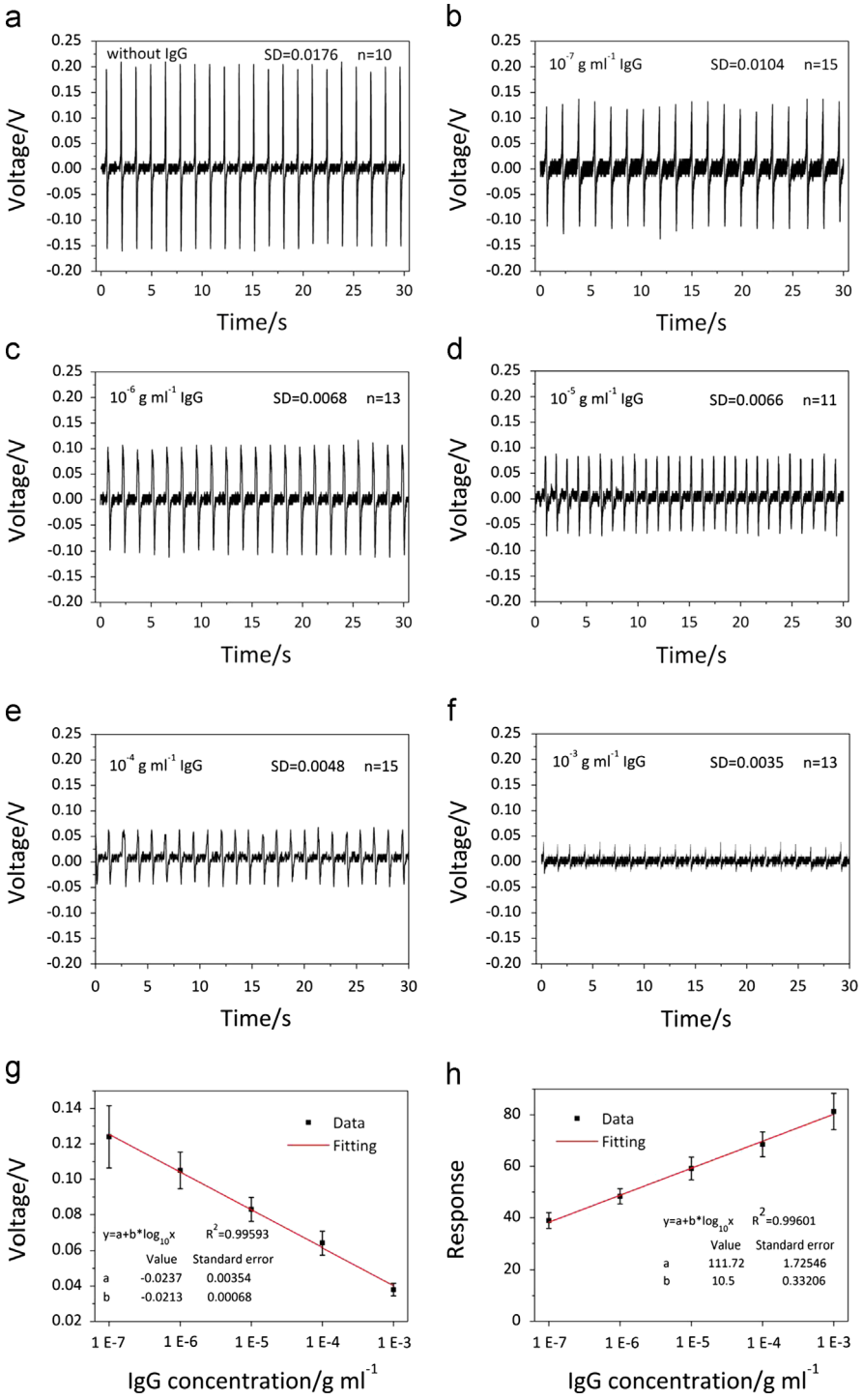

Fig. 4. The piezoelectric output of the device after being immersed in different concentrations of IgG solution. (a) None IgG, (b) 10^{-7} g ml^{-1}, (c) 10^{-6} g ml^{-1}, (d) 10^{-5} g ml^{-1}, (e) 10^{-4} g ml^{-1}, (f) 10^{-3} g ml^{-1}, (g) the relationship between the piezoelectric output of the device and the concentration of IgG, and (h) the dependence of the response r on the concentration of IgG.

Table 1
The LODs of the different detection methods and the references.

Detection method	LOD (ng ml^{-1})	Reference
Self-powered active biosensing	6.9	This work
Electrochemical with microfluidic	10	Dong et al. (2007)
Electrochemical with polyaniline	3	Lee et al. (2011)
Quartz crystal microbalance	3.5	Chu et al. (2006)
Surface plasmon resonance	7.5	Wang et al. (2010)

(LOD; the signal to noise ratio (SNR) is 3:1 (Toribio et al., 2002; Field and Reed, 1996)) can be calculated to be about 6.9 ng ml^{-1} using the fitted linear equation in Fig. 4g. Many other methods have been reported for detecting IgG molecules, such as electrochemical, quartz crystal microbalance (QCM) and surface plasmon resonance (SPR). The comparison of LODs between these methods and our result is shown in Table 1.

Similar to the definition of response (r) of transistor-type biosensor ($r = (|I_0 - I_i|/I_0) \times 100\%$, where I_0 and I_i are the currents

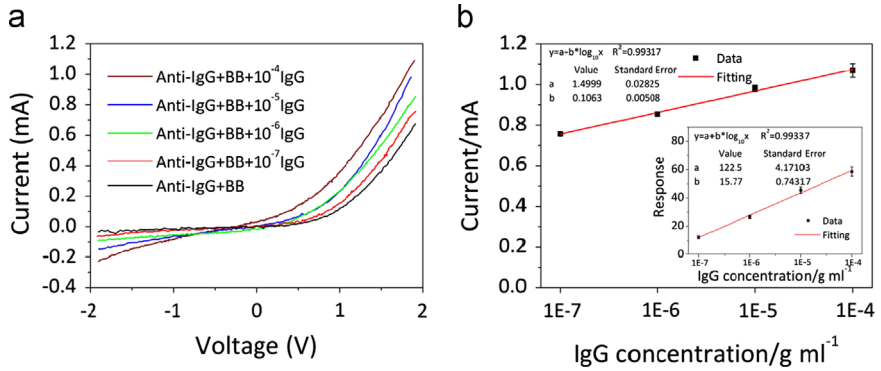

Fig. 5. (a) The *I–V* curves of one device in different concentration of IgG without applied deformation. (b) Current response of the device at a fixed voltage of 1.9 V without applied deformation. The inset shows the response of the device with different concentrations of IgG.

of the sensor without IgG and with IgG, respectively) (Yu et al., 2013a), the response (a voltage variation in function of the concentration of IgG) of the self-powered active biosensor can simply be defined as

$$r = \frac{|V_0 - V_i|}{V_0} \times 100\% \quad (1)$$

where V_0 and V_i are the piezoelectric output without IgG and with IgG, respectively. The responses against 10^{-7}, 10^{-6}, 10^{-5}, 10^{-4} and 10^{-3} g ml^{-1} IgG are about 38.9 ± 3.06, 48.3 ± 2.94, 59.1 ± 4.42, 68.5 ± 4.83 and 81.3 ± 7.04, respectively (shown in Fig. 4h). And the RSD ranges from 6.08% to 8.66%.

As discussed above, the free-carrier density inside ZnO NWs plays a crucial role in affecting the output of the NG, and the adsorption of IgG can increase the carrier density in NWs by a "floating gate" effect. Such a change of charge–carrier density can be directly demonstrated by the resistance of the ZnO NWs. Fig. 5a shows the room-temperature *I–V* curves of one NG without deformation. There is a typical metal–semiconductor–metal (M–S–M) structure in our device (Al–ZnO–Ti). The nonlinear *I–V* characteristic is caused by the asymmetric Schottky barrier heights formed between ZnO NWs and the two metal electrodes (Zhang et al., 2011). Compared with the curve of the NG without IgG functionalization, the *I–V* curves shift upwards when the device has been immersed in IgG. As the concentration of IgG increases, the resistance of the device decreases, further confirming that the change of carrier density in ZnO NWs arises from the adsorption of IgG. Under the applied bias voltage of 1.9 V, the currents of the device are 0.674 ± 0.0140, 0.757 ± 0.0047, 0.854 ± 0.0099, 0.981 ± 0.0154 and 1.069 ± 0.0328 mA with the IgG concentrations of 0, 10^{-7}, 10^{-6}, 10^{-5}, and 10^{-4} g ml^{-1}, respectively, as shown in Fig. 5b (test number $n=5$). And the RSD ranges from 0.62% to 3.06%. This behavior can be treated as a transistor-type biosensor (*I–V* behavior). The response against 10^{-7}, 10^{-6}, 10^{-5}, and 10^{-4} g ml^{-1} IgG is 12.3 ± 0.96, 26.7 ± 1.26, 45.5 ± 2.26 and 58.6 ± 3.27, respectively, as shown in the inset of Fig. 5b. The RSD ranges from 4.72% to 7.80%. Higher response is obtained from the new piezo-biosensing device compared with the transistor-type biosensor (*I–V* behavior), suggesting that biomolecule-adsorption-dependent piezoelectric output of the new device has great potential for realizing high-response biosensing. However, with the same concentration of IgG, the response of the new device is still lower than the results in the previous reports (Yu et al., 2013b; Mao et al., 2010). And the sensitivity of the new device is about 10.5 (the slope of the fitted line in Fig. 4h), lower than the results in the previous literatures (Yu et al., 2013b; Mao et al., 2010). Thus further work needs to be done on enhancing the response and the sensitivity of the new device.

4. Conclusion

In summary, self-powered active biosensor has been realized from ZnO NW NG. The piezoelectric output generated by ZnO NW NG can act not only as a power source for driving the device, but also as a biosensing signal. The biosensing response of the new device is high, and the LOD on IgG is about 6.9 ng ml^{-1}. The present results demonstrate a feasible approach for actively detecting biomolecules by coupling the piezotronic and biosensing characteristics of ZnO NWs. Our work can also stimulate a research trend on designing new device structures and material systems for the future development of self-powered active biosensors.

Acknowledgments

This work was supported by the National Natural Science Foundation of China (51102041 and 11104025), the Fundamental Research Funds for the Central Universities (N120205001, N120405010 and lzujbky-2013-35), and Program for New Century Excellent Talents in University (NCET-13-0112).

References

Besteman, K., Lee, J.O., Wiertz, F.G.M., Heering, H.A., Dekker, C., 2003. Nano. Lett. 3 (6), 727–730.
Cai, H., Xu, C., He, P., Fang, Y., 2001. J. Electroanal. Chem. 510 (1), 78–85.
Chen, X.-Y., Li, J.-R., Li, X.-C., Jiang, L., 1998. Biochem. Biophys. Res. Commun. 245 (2), 352–355.
Chu, X., Zhao, Z.-L., Shen, G.-L., Yu, R.-Q., 2006. Sens. Actuators B: Chem. 114 (2), 696–704.
Cui, Y., Wei, Q.Q., Park, H.K., Lieber, C.M., 2001. Science 293 (5533), 1289–1292.
Curreli, M., Li, C., Sun, Y.H., Lei, B., Gundersen, M.A., Thompson, M.E., Zhou, C.W., 2005. J. Am. Chem. Soc. 127 (19), 6922–6923.
Dennison, M.J., Turner, A.P.F., 1995. Biotechnol. Adv. 13 (1), 1–12.
Dong, H., Li, C.-M., Zhang, Y.-F., Cao, X.-D., Gan, Y., 2007. Lab Chip 7 (12), 1752–1758.
Dong, X., Shi, Y., Huang, W., Chen, P., Li, L.-J., 2010. Adv. Mater. 22 (14), 1649–1653.
Field, J.A., Reed, R.L., 1996. Environ. Sci. Technol. 30 (12), 3544–3550.
Gao, Y., Wang, Z.L., 2009. Nano Lett. 9 (3), 1103–1110.
Gui, E.L., Li, L.-J., Zhang, K., Xu, Y., Dong, X., Ho, X., Lee, P.S., Kasim, J., Shen, Z.X., Rogers, J.A., Mhaisalkar, S.G., 2007. J. Am. Chem. Soc. 129 (46), 14427–14432.
He, J.H., Zhang, Y.Y., Liu, J., Moore, D., Bao, G., Wang, Z.L., 2007. J. Phys. Chem. C 111 (33), 12152–12156.
Heller, I., Janssens, A.M., Mannik, J., Minot, E.D., Lemay, S.G., Dekker, C., 2008. Nano Lett. 8 (2), 591–595.
Hu, Y., Lin, L., Zhang, Y., Wang, Z.L., 2012. Adv. Mater. 24 (1), 110–114.
Hu, Y.F., Zhou, J., Yeh, P.H., Li, Z., Wei, T.Y., Wang, Z.L., 2010. Adv. Mater. 22 (30), 3327–3332.
Lee, I., Luo, X., Cui, X.T., Yun, M., 2011. Biosens. Bioelectron. 26 (7), 3297–3302.
Lee, M., Bae, J., Lee, J., Lee, C.-S., Hong, S., Wang, Z.L., 2011b. Energy Environ. Sci. 4 (9), 3359–3363.
Li, L., Huang, J., Wang, T., Zhang, H., Liu, Y., Li, J., 2010. Biosens. Bioelectron. 25 (11), 2436–2441.
Li, Z., Huang, X., Liu, J., Li, Y., Li, G., 2008. Mater. Lett. 62 (10), 1503–1506.
Lieber, C.M., 2003. MRS Bull. 28 (7), 486–491.
Mao, S., Lu, G., Yu, K., Bo, Z., Chen, J., 2010. Adv. Mater. 22 (32), 3521–3526.

Maroto, A., Balasubramanian, K., Burghard, M., Kern, K., 2007. ChemPhysChem 8 (2), 220–223.
Mello, L.D., Kubota, L.T., 2002. Food Chem. 77 (2), 237–256.
Pan, C., Li, Z., Guo, W., Zhu, J., Wang, Z.L., 2011. Angew. Chem. 123 (47), 11388–11392.
Pan, C., Yu, R., Niu, S., Zhu, G., Wang, Z.L., 2013. ACS Nano 7 (2), 1803–1810.
Patolsky, F., Lieber, C.M., 2005. Mater. Today 8 (5), 20–28.
Rembaum, A., Dreyer, W., 1980. Science 208 (4442), 364–368.
Song, Y.J., Qu, K.G., Zhao, C., Ren, J.S., Qu, X.G., 2010. Adv. Mater. 22 (19), 2206–2210.
Toribio, F., Moyano, E., Puignou, L., Galceran, M., 2002. J. Chromatogr. A 948 (1), 267–281.
Wang, Y., Huang, C.-J., Jonas, U., Wei, T., Dostalek, J., Knoll, W., 2010. Biosens. Bioelectron. 25 (7), 1663–1668.
Wang, Z.L., 2010. Nano Today 5 (6), 540–552.
Wang, Z.L., 2012. Adv. Mater. 24 (34), 4632–4646.
Wang, Z.L., Song, J.H., 2006. Science 312 (5771), 242–246.
Wu, H.C., Peng, Y.C., Shen, T.P., 2012. Materials 5 (11), 2088–2100.
Xu, S., Qin, Y., Xu, C., Wei, Y., Yang, R., Wang, Z.L., 2010. Nat. Nanotechnol. 5 (5), 366–373.
Xue, X.Y., Nie, Y.X., He, B., Xing, L.L., Zhang, Y., Wang, Z.L., 2013. Nanotechnology 24 (22), 225501–225506.
Yang, R., Qin, Y., Dai, L., Wang, Z.L., 2008. Nat. Nanotechnol. 4 (1), 34–39.
Yeh, P.H., Li, Z., Wang, Z.L., 2009. Adv. Mater. 21 (48), 4975–4978.
Yu, R., Pan, C., Chen, J., Zhu, G., Wang, Z.L., 2013a. Adv. Funct. Mater. 23 (47), 5868–5874.
Yu, R., Pan, C., Wang, Z.L., 2013b. Energy Environ. Sci. 6 (2), 494–499.
Zhang, F., Ding, Y., Zhang, Y., Zhang, X., Wang, Z.L., 2012a. ACS Nano 6 (10), 9229–9236.
Zhang, R., Lin, L., Jing, Q., Wu, W., Zhang, Y., Jiao, Z., Yan, L., Han, R.P.S., Wang, Z.L., 2012b. Energy Environ. Sci. 5 (9), 8528–8533.
Zhang, Y., Liu, Y., Wang, Z.L., 2011. Adv. Mater. 23 (27), 3004–3013.